EVLA Memo 117

Ionospheric Effects and Calibration
of the VLA at 327 MHz

W. D. Cotton, Juan. M. Uson
NRAO [1]

Abstract

Ionospheric electron density variations cause time and position variable refraction of sources seen through the medium. In extreme cases, i.e. at low frequencies, this can also defocus the image of the sky. This study investigates the effects of position and time variable ionospheric refraction on VLA observations at 327 MHz. The field–based technique of [3], [1] developed for use at 74 MHz is applied for correction of high resolution observations at 327 MHz. The result is improved imaging although some artifacts remain. Examples are shown using the Obit (http://www.cv.nrao.edu/∼bcotton/Obit.html) package.

Contents

List of Figures

1 Introduction

Electromagnetic signals propagating through an ionized medium experience an excess phase delay proportional to the frequency to the -2 power and can be a serious source of phase corruptions for radiation at low frequencies. The Earth's ionosphere is such an ionized medium and its irregularities have long been recognized as the major source of phase errors for high resolution arrays at frequencies below ~100 MHz. However, since the resolution of an array is proportional to the frequency, the effects of ionospheric phase corruptions on derived images only drop as the frequency to the negative first power.

This study investigates the effects of ionospheric irregularities on data at higher frequencies, namely 327 MHz, and the efficacy of the technique developed for lower frequencies, the field–based technique of [3], [1]. The field–based calibration technique is applied to a deep observation of a field with the VLA in A configuration. Data processing described in this memo used the Obit (http://www.cv.nrao.edu/~bcotton/Obit.html) package.

2 Field–Based Calibration

An electromagnetic wavefront passing through a medium of variable index of refraction will experience variable phase delays in different parts of the wavefront. A wedge in the density of such a medium will cause a linear gradient across an array observing through such a medium resulting in a refraction of any objects viewed. Higher order variations in the index of refraction will cause a more serious distortion of the wavefront producing defocusing and scintillations in extreme cases. Calibration of interferometric arrays involves estimating and correcting these phase effects.

The traditional antenna–based calibration is designed to model phase corruptions largely due to variations in tropospheric water vapor density. This case is illustrated in cartoon form in Figure 1 where it is seen that the phase screen is quite close to the antennas so that the phase errors are largely uncorrelated between antennas. Also, since the phase screen is so close to the antenna, the phase errors at each antenna will be correlated over large areas of the sky. Thus, a single phase shift per antenna suffices to describe the tropospheric phase corruptions.

On the other hand, the ionosphere is at a much greater height, from about 100 km to several hundred km and is illustrated in the cartoon in Figure 2. In this case, the phase corruptions are highly correlated between antennas but vary with angle on the sky. Thus, the "isoplanatic" patch size may be smaller than in the case of tropospheric phase errors. Ionospheric phase errors are not well described by a single phase per antenna but are better described by a phase screen across the array.

In the regime that the phase screen can be adequately described as a linear gradient across the array for a wavefront coming from any given direction, the image of a small source will not be distorted or defocused, but will appear shifted from its actual position. This apparent position shift may vary across the field of view of the array elements. In this regime, the "field–based" method of [3], [1] is applicable. This technique is to make a series of snapshot measurements around the locations of known strong sources in the field, deconvolve the images, and estimate the apparent offsets of each. The time sequence of the derived set of apparent source position offsets allows the fitting of a time variable geometric distortion of the sky as seen by the array. Low order Zernike polynomials are a useful set of functions for modeling the distortion field. The field is modeled as a phase screen and each position offset measurement gives a 2-D gradient in this screen at the puncture point of the line of sight to the calibrator. Due to the paucity of usable calibrators in VLA 74 MHz observations, only a 5 term Zernike model is used. This allows a 2D gradient in position offsets across the field of view. There is no simple operation that can "calibrate" the data due to the spatial dependence of the correction. The time variable geometric distortion model must be used in the imaging and deconvolution process to apply corrections.
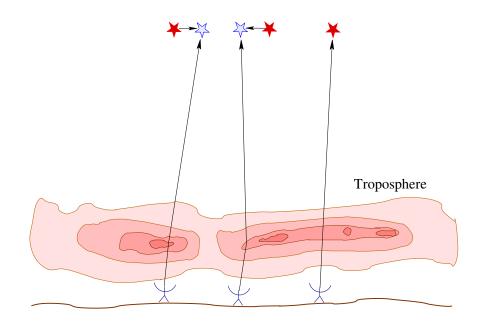
Figure 1: A cartoon view of the troposphere over an interferometer array. The shading shows the relative index of refraction and the lines show the effects on the apparent direction to the source. The tropospheric refraction causes relatively independent apparent deflections of source positions among the various antennas. Since the phase screen is so close to each antenna, a large area of the sky is viewed through the same portion of the phase screen.
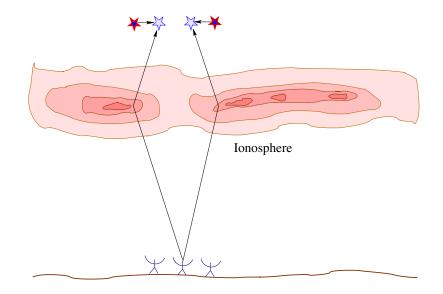

Figure 2: A cartoon view of the ionosphere over an array. The shading shows relative values of the index of refraction and the lines show the effects on the apparent direction to the source. Each element of the array looks through nearly the same portion of the ionosphere towards a given source but the portion of the ionosphere varies between sources.

At low frequencies with 2-D arrays, some provision must be made for the curvature of the sky. One solution to this problem is the "Fly's eye" approach where the sky is tiled with many small facets, each tangent to the celestial sphere at its center. In practice, the size of the tile needed is smaller than the isoplanatic patch size (or at least the resolution at which the phase screen can be determined), so a sufficient approximation to dedistorting the sky is to correct each facet for the ionospheric offset at its center. This is done by calculating the antenna–based phase corrections at the center of the facet and applying these corrections prior to deriving the dirty image (or residual) of that facet. If a visibility–based deconvolution is used, the apparent positions of the CLEAN components need time dependent corrections, before Fourier transforming, to reintroduce the distortions into the model. More details of Field–Based calibration are given in [2].

3 Application to 327 MHz

3.1 Modifications to 74 MHZ Practice

Ionospheric phase corruptions at 327 MHz at the VLA are seldom, if ever, sufficiently severe to defocus the image so an initial self–calibration is an adequate precursor to field–based calibration.

At 327 MHz the galactic background is far weaker than at 74 MHz, resulting in greatly increased sensitivity, and the ionospheric coherence time is longer. Thus, there are many more detectable calibrators in the field of view in a coherence time. This means that a more complex model than a 5 term Zernike polynomial is possible.

Since initial imaging using self–calibration is possible, a calibrator catalog can be derived from the self–calibrated image. This catalog will contain only sources know to be detectable so some of the filtering to remove false calibrator detections can be relaxed.

3.2 Example

To test the application of field–based calibration to VLA 327 MHz data, it was applied to a deep integration ($\sim$ 12 hours) observations of a field in the A configuration. This data was fully self calibrated prior to field–based calibration. A catalog of 40 bright sources visible in the self–calibrated image was generated for use in the subsequent calibration. The self–calibration will remove any common position offsets due to ionospheric refraction.

The ionospheric calibration used the Obit task IonCal. In the ionospheric calibration a ten term Zernike polynomial was used although it produced only marginally lower residuals than a five term fit.

The distribution on the sky of the calibration sources and the observed offsets and residuals from the fitted ionospheric model are shown in Figures 3 and 4. At the beginning and end of the observations, when the field was observed at low elevation, the offsets are large, the distortion pattern complex and the fits relatively poor. During the middle of the observations, when the source was at higher elevations, the offsets are smaller and the fitting better. The observations were interrupted by a snow storm, and at the end the antennas had some snow loading.

Another way to view the success of the ionospheric modeling is a time series of position offsets for individual calibrators. Several such plots are shown in Figures 5 and 6. Calibrator 20 is the strongest source in each snapshot image so has the highest weight in the fitting. Calibrator 40 is near the null in the primary antenna pattern which likely explains its bizarre behavior. The instability possible in this 10 term polynomial series is apparent in the wild variations of the model fit towards the end of the observations.

The best measure of success of the technique is its effect on the images. Imaging without ionospheric calibration used the Obit task Imager, and imaging with ionospheric calibration used the Obit task IonImage. Comparison images with and without ionospheric corrections for several
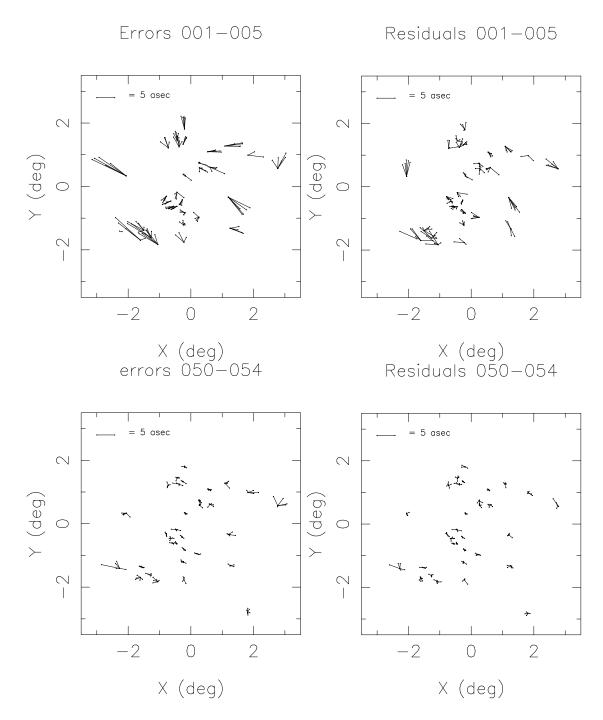
Figure 3: **Top:** Positions of sources plotted on the Zernike plane with position offsets, multiplied by 500, for 5, three–minute solutions at the beginning of the observations. Lines are drawn between the actual position and the apparent position for each solution. On the left are the observed offsets and on the right are the offsets after correction by the fitted Zernike polynomial. A 5 arc second scale bar is given on the top left of each plot.
Bottom: As for top but for solutions well into the observations.

errors 100−105

Residuals 100−105

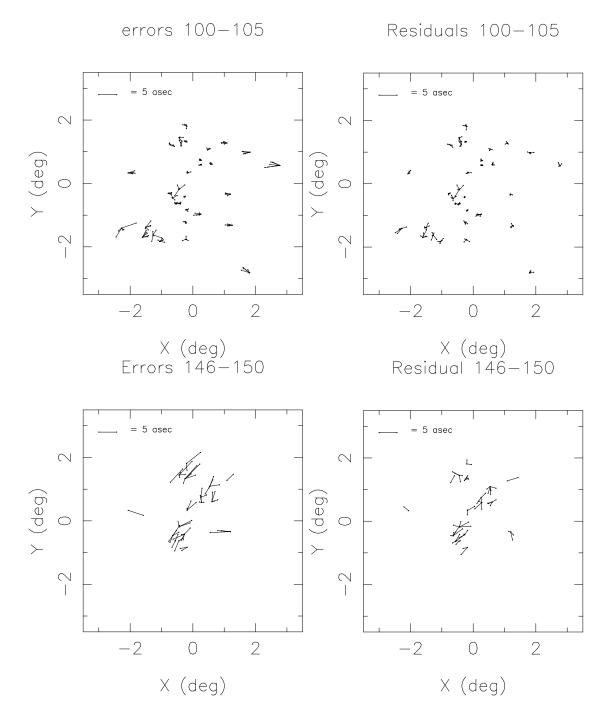Errors 146−150

Residual 146−150

Figure 4: **Top:** As for Figure 3 but for solutions well into the observations.
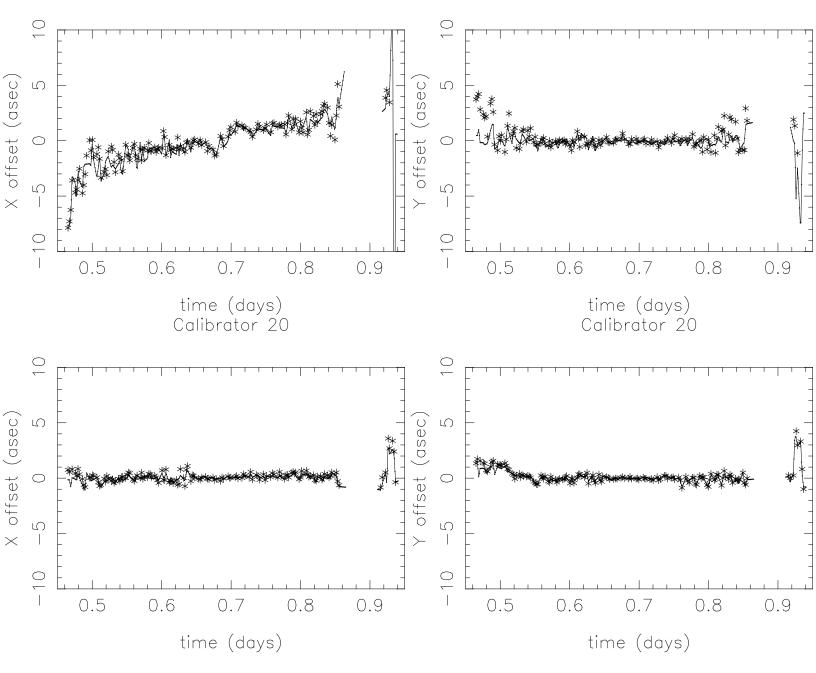**Bottom:** As for Figure 3 but for solutions at the end of the observations.

Figure 5: **Top:** Measured offsets and Zernike model values for Calibrator 2 as a function of time. The *s indicate measurements and the solid line is the sequence of models fitted to all calibrators. X (RA) offset on the left, Y (Dec) offset on the right.
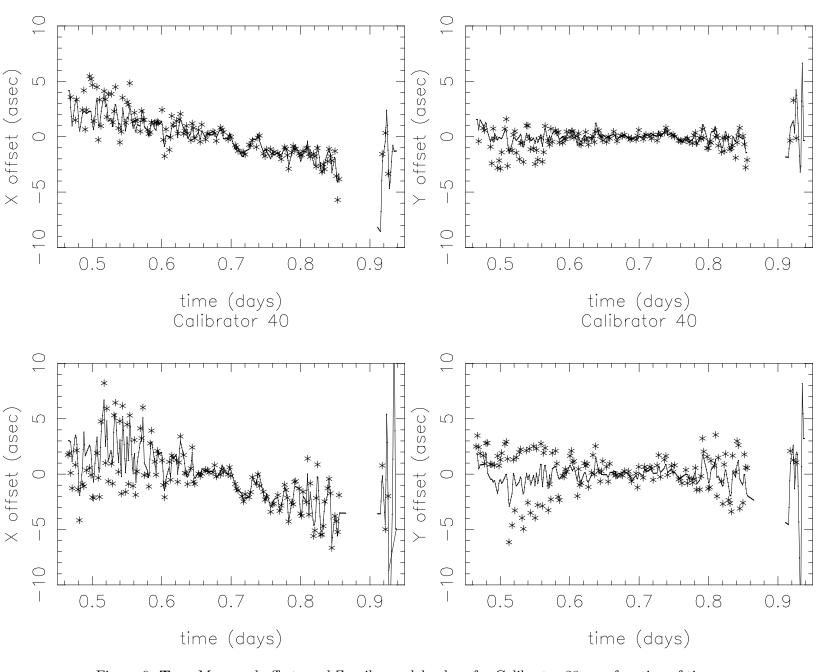**Bottom:** As for **Top:** but for Calibrator 20.

Figure 6: **Top:** Measured offsets and Zernike model values for Calibrator 38 as a function of time. X (RA) offset on the left, Y (Dec) offset on the right.
Bottom: As for **Top:** but for Calibrator 40. Note: this source is near the null in the antenna pattern.

of the strongest sources in the field are given in Figure 7. The procedure significantly reduced but did not completely eliminate the artifacts seen around the brightest sources.

4   Conclusions

In the above, we have shown that under at least some observing conditions, the quality of images derived from VLA 327 MHz data is limited by ionospheric corruptions and that applying the technique derived for VLA 74 MHz data significantly improves the results. Similar tests on data provided by Frazer Owen show a lower level of ionospheric activity and the artifacts in the images are dominated by other effects, probably the non-circularity of the antenna patterns.

In the data studied here, the accuracy of the ionospheric modeling appears limited by the basis set, Zernike polynomials, used. A better model is needed for the phase screen.

5   Acknowledgments

References

[1] W. D. Cotton. Lessons from the VLA Long Wavelength Sky Survey (VLSS). In *Science with Human Wavelengths, Astronomical Society of the Pacific Conference Series, vol, 345*, pages 337–340, 2005.

[2] W. D. Cotton. Ionospheric Effects and Imaging and Calibration of VLA Data. *EVLA Memo 118*, ftp://ftp.cv.nrao.edu/NRAO-staff/bcotton/Obit/IonImage.pdf:1–12, 2007.

[3] W. D. Cotton, J. J. Condon, R. A. Perley, N. Kassim, J. Lazio, A. Cohen, W. Lane, and W. C. Erickson. Beyond the isoplanatic patch in the VLA Low-frequency Sky Survey. In *Proceedings of the SPIE, Volume 5489.*, pages 180–189, 2004.
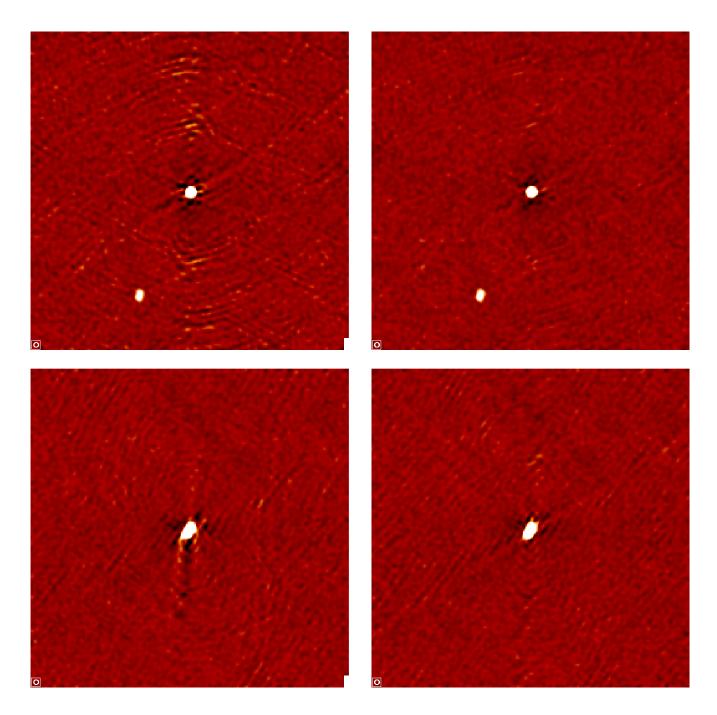
Figure 7: **Top:** Comparison of the region around the brightest source in the field (Calibrator 20) showing pixel range -4 to 10 mJy/beam. On the left is the uncorrected image (peak 336 mJy/beam) and on the right the corrected image (peak 348 mJy/beam). The resolution is shown in the lower left of each plot. The source is 1.35 degrees from the pointing center.
Bottom: As for **Top:** but for another source. Uncorrected peak 145 mJy/beam, corrected 153 mJy/beam. The source is 1.63 degrees from the pointing center.